Pneumatic Conveying of Granular Solids in Horizontal and Inclined Pipes

Kewu Zhu and Chun Kit Wong
Dept. of Chemical and Environmental Engineering, National University of Singapore, Singapore 117576

S. Madhusudana Rao
MEBCS Program, Singapore–MIT Alliance, Singapore 117576

Chi-Hwa Wang
Dept. of Chemical and Environmental Engineering, National University of Singapore, Singapore 117576

and

MEBCS Program, Singapore–MIT Alliance, Singapore 117576

DOI 10.1002/aic.10172
Published online in Wiley InterScience (www.interscience.wiley.com).

Computational fluid dynamics simulations are used to investigate the pneumatic conveying of granular solids through an inclined pipe at different inclinations. Model predictions agreed reasonably well with the measurements reported by Tsuji and Morikawa in 1982 for mean gas and solids velocities. The results of influence of model parameters, inclination angle, and feeding conditions on the flow patterns were also reported. Particle–wall collisions were found to have a very significant effect on the solids distribution over the cross section of the conveying tube for large particles. Upon introducing finite-amplitude sinusoidal fluctuations in the gas velocity at the inlet of the pipe, solids density waves were observed to move along the conveying line with significant axial dispersions. © 2004 American Institute of Chemical Engineers *AIChE J,* 50: 1729–1745, 2004

Keywords: pneumatic conveying, mathematical model, granular materials, powder technology, simulation

Introduction

Turbulent gas-solid flows have many applications in industrial equipment such as cyclone separators, chemical reactors, fluidized beds, and pneumatic transport systems. These systems often involve complicated flow dynamics and interactions between flow constituents and their surroundings. To achieve efficient operation and optimum design of these systems, it is essential to understand the flow dynamics in gas-solid flow systems.

In horizontal pneumatic transport of granular solids, the flow features are very complicated because of the action of gravitational forces perpendicular to the flow direction (Owen, 1969). The solids distribution over the cross section of the conveying pipe is substantially influenced by gravitational forces, gas-phase turbulence, collision between particles, and collision between particles and the wall (Huber and Sommerfeld, 1994; Lun and Liu, 1997; Tsuji and Morikawa, 1982) when particles are transported in a horizontal/inclined tube by a turbulent gas stream. Tsuji and Morikawa (1982) used a

Correspondence concerning this article should be addressed to C.-H. Wang at chewch@nus.edu.sg.

laser-Doppler velocimeter (LDV) to measure the gas and solids velocities of the two-phase flow in a horizontal pipe (diameter = 30.5 mm). They found that the gas-phase velocity profiles were flattened because of the presence of particles and the degree of flatness was enhanced with increasing solids mass loading. They also observed that velocity profiles of both gas and solids phases exhibited asymmetric distribution attributed to the action of gravity. Kussin and Sommerfeld (2001) used phase-Doppler anemometry (PDA) to investigate the effect of particle size (diameters ranging from 60 to 1000 μm), solids mass loading (m, defined as solid mass flow rate/gas mass flow rate, <2.0), and wall roughness on the flow behavior of a gas-solid mixture in a horizontal channel. The results obtained were similar to those reported by Tsuji and Morikawa (1982). Huber and Sommerfeld (1994) measured the solids concentration distribution over the cross section of the pipe along the conveying line. They investigated the influence of various parameters such as wall roughness, conveying velocity, and solids mass loading on the solids concentration distribution. Our recent experimental studies (Rao et al., 2001; Zhu et al., 2003) on the pneumatic conveying of horizontal and inclined pipes, using electrical capacitance tomography (ECT) measurements, revealed the existence of density waves even in the visually classified homogeneous flow regime. From the power spectra of single-plane ECT concentration fluctuation data (also confirmed by the periodic secondary peaks in the cross-correlation data of twin-plane measurements), these density waves were attributed to feeding disturbances. However, it was not clear how these inlet disturbances propagate along the conveying line. In the present work, numerical simulations were carried out to examine the propagation of disturbances by adding solid and air feed rate perturbations at the inlet of the conveying pipe and then probing their spatial and temporal variations.

Apart from horizontal and vertical pneumatic conveying systems, inclined pneumatic conveying lines are quite common in industry and thus attract attention among researchers. Levy et al. (1997) investigated the pressure drop in inclined pneumatic conveying systems by both experiments and numerical simulation. Hirota et al. (2002) experimentally studied the influence of mechanical properties of powders on pressure drops in inclined gas-solid flows. Although most of these investigations were focused on pressure drop information, little work has been found in the literature that entails various aspects of inclined pneumatic conveying of solids.

Numerical simulations play a significant role in the understanding of the dynamics of gas-solid flows and in the prediction of the flow behavior of such systems. Computational fluid dynamics (CFD) is becoming a powerful tool used to study two-phase flows as the result of rapid advances in computational capabilities. In the framework of Eulerian approaches, the solids phase is commonly modeled using grain kinetic theory, given the importance of particle–particle collisions in pneumatic conveying systems (Bolio et al., 1995; Louge et al., 1991). Sinclair and Jackson (1989) analyzed fully developed gas-solid flow in a vertical pipe where interactions between solid particles were dominated by solid bicollisions. Ocone et al. (1993) extended the work of Sinclair and Jackson (1989) on the gas-solid laminar flow in a vertical tube to an arbitrarily inclined duct. Because in most pneumatic conveying systems the motion of the gas phase is very likely to be vigorously turbulent and will significantly affect the flows, quantitative predictions are unlikely to be obtained from models not including gas-phase turbulence (Ocone et al., 1993). In Ocone et al. (1993), the interaction forces considered for the solids consisted of the collision force between particles and the mutual drag force between the gas and solid phases (two-way coupling) and the simulation was based on one-dimensional (1-D) fully developed channel flows.

Numerical studies on vertical gas-solid flows are commonly presented in the literature. In contrast, only a few numerical studies have been reported on the horizontal and inclined pneumatic conveying of granular solids. Moreover, previous studies on dilute phase gas-solid flow used a two-fluid model, using only very fine particles whose motion is controlled by the gas phase.

In the present work, we examine the flow behaviors associated with relatively large particles, in which particle motion is largely affected by particle–particle and particle–wall collisions. Furthermore, gas-phase turbulence is incorporated into the model proposed by Ocone et al. (1993) to study the horizontal, inclined, and vertical pneumatic conveying of solids. The flow considered is within the relatively dilute regime ($m < 7$, maximum solid concentration $< 10\%$) so that solid stress is dominated by solid bicollision and translation, whereas frictional contribution to the solid stress is negligible. The various types of interactions between the gas and solids are considered as four-way coupling in three-dimensional (3-D) pipe flows: (1) effect of particles on gas-phase mean-flow field; (2) particle–particle interactions; (3) presence of particles on gas-phase turbulence; (4) gas-phase turbulence on the motion of particles.

The CFD model is to be validated using established experimental data reported by Tsuji and Morikawa (1982). Subsequently, the influences of model parameters, pipe inclinations, and feeding conditions on the flow behavior are investigated. Novelties of the present work are given by the following:

(1) In contrast to other similar studies (Louge et al., 1991; Ocone et al., 1993; Sinclair and Jackson, 1989) dealing with fully developed flows, full scale 3-D transient pneumatic conveying of granular solids was investigated.

(2) Gas-phase turbulence was believed to be critical for the numerical investigation of dilute-phase transport. The influence of gas-phase turbulence on the flow features was evaluated numerically.

(3) According to Rao et al. (2001) and Zhu et al. (2003) disturbances resulting from the feeders significantly influence the solids feed rate. The effects of such disturbances on flow features were numerically investigated by introducing various perturbations at the feed end.

(4) Particle–particle and particle–wall interactions are believed to be very important in dilute pneumatic conveying systems. Systematic analysis of influences of these interactions on flow features was presented. The results obtained could provide an explanation to flow nonuniformities in a horizontal conveying line and may be useful for better understanding of solids clustering and the dynamics of pneumatic conveying systems.

Mathematical Model

Anderson and Jackson (1967) developed the governing equations for gas-solid mixture using a continuum approach.

By a volume-averaging approach, the equations for the gas- and solid-phase mass and momentum balance are obtained. In such a formulation, the point hydrodynamic variables are replaced by local averaged variables describing the processes on a scale larger than particle size but smaller than the system dimensions. In the present work, we used the software package Fluent to study the pneumatic conveying system. The solid phase was modeled using grain kinetic theory (Bolio et al., 1995; Lun et al., 1984; Sinclair and Jackson, 1989), together with boundary conditions of granular temperature and solid slip velocity developed by Johnson and Jackson (1987). The gas phase was modeled using a modified high-Reynolds number model together with the standard wall function (Lauder and Spalding, 1974).

Active research has recently been carried out on the turbulence–particle interactions. Kenning and Crowe (1997) proposed a model for turbulence modulation for gas-particle flows based on the work done by particle drag and the dissipation based on a length scale corresponding to the interparticle spacing. Sato et al. (2000) experimentally investigated the influence of interparticle spacing on the distortion of turbulence using particle-image velocimetry. Peirano and Leckner (1998) and Peirano et al. (2002) modeled the turbulence modulation considering the work of forces exerted on the particles as the particles move in the turbulent field, whereas the effect of the velocity fluctuations produced by the wakes is not considered. For a relatively large particle considered in the current work, turbulence modulation attributed to wakes may be important. Yuan and Michaelides (1992) proposed a mechanistic model based on wake shedding for turbulence generation. Mallo (1997) further improved the model of Yuan and Michaelides by proposing an empirical formula based on Schwartz's inequality to investigate the turbulence modulation. Mallo (1997) found that this empirical formula can provide reasonably good agreement with experimental results. For simplicity, Mallo's empirical formula is used in the present study, although detailed discussion and evaluation of different turbulence–particle interactions are beyond the scope of this article. The 3-D model equations as well as boundary conditions used in this work are summarized in the Appendix.

The simulations are carried out using a nonorthogonal boundary-fitted coordinate grid system. The set of coupled conservation equations were discretized into systems of linear equations using the finite-volume method on the nonorthogonal grids. The discretization on nonorthogonal grids can be found in Coelho and Pereira (1993) and Lien et al. (1996). The discretization of the convection terms in the momentum equations uses the power-law interpolation scheme (Patankar, 1980), which provides solutions with an accuracy between that obtained from first- and second-order schemes. Compared with other higher-order schemes, this method is more robust and less computationally intensive. The discretization scheme for time is fully implicit, which eliminates the time-step constraints in the integration. Taking advantage of the strong coupling between pressure and velocity, the SIMPLE (semi-implicit method for pressure link equations) iterative algorithm relates the pressure and velocity correction to recast the continuity equation in terms of a pressure-correction equation (Patankar, 1980). Underrelaxation factors were necessary to obtain convergent solutions with the iterative scheme used. Relaxation factors used in the current study had typical values of 0.2 for air and solid velocities, solid volume fraction, granular pressure, gas turbulence kinetic energy, and dissipation rate of kinetic energy; and 0.25 for granular temperature and gas pressure. The solution is assumed to converge when the sum of normalized residuals has fallen below a specified level δ

$$\frac{\sum_{CV} |R_\Phi|}{\sum_{CV} |\Phi|} < \delta \tag{1}$$

where R_Φ is the local residual of the Φ equation, Φ is the corresponding local quantity, and subscript CV denotes the control volume. In the present study, δ is assigned as 0.001. The set of conservation equations were solved using the software package Fluent. Simulations were monitored to ensure converged solutions at each time step. The grid-independence studies were carried out to ensure sufficient spatial resolutions. Mass balance was verified to ensure convergence.

Results and Discussion

Figure 1 shows the geometry used for the simulation. The X–Y plane denotes the cross section of the conveying tube, whereas Z and θ represent the axial direction and inclination angle (defined as the angle between the pipe and horizontal line), respectively. To compare model predictions with experimental data, the simulated flow quantities are taken at a fully developed region along a center line L at station A with distance of Z_L from the solids feeding end. The parameter values of the turbulence model used in the present study are summarized in Table 1.

Grid-independence study

To obtain accurate numerical results, grid-independence investigation is necessary. In this section, we present only the influence of grid size on numerical prediction at conveying velocity $U = 15.6$ m/s, solids mass flux $G_s = 49.7$ kg/(m^2·s) under horizontal conveying ($\theta = 0°$) of 2.8-mm particles.

Agrawal et al. (2001) demonstrated that coarse grid simulation averaged out the mesoscale structures and these unresolved structures (solids clusters/mesoscale structures) had significant effects on flow features occurring on scales larger than the grid size. To accurately predict the gas-solid flow behaviors, it is necessary to resolve the mesoscale structures that afford a significant contribution to the macroscale flow behaviors (Agrawal et al., 2001; Zhang and VanderHeyden, 2001). Zhang and VanderHeyden (2001) claimed that it was necessary to adopt a very fine grid scheme to obtain grid-independent results. A series of studies at various grid schemes [(a) $200 \times 6 \times 6$, (b) $300 \times 8 \times 8$, (c) $400 \times 10 \times 10$, and (d) $800 \times 12 \times 12$] were carried out to ensure sufficient spatial resolution. Pressure gradient, solids mass flux, and solids volume fraction distribution were chosen to evaluate the influence of the grid scheme on the numerical solutions.

Figure 2(i) shows the effects of grid scheme on the solids mass flux profiles detected at the central control volumes along the conveying tube. Detected mass fluxes decreased with decreasing grid sizes down to that used in grid scheme c, $400 \times 10 \times 10$. There was not much difference in the mass fluxes

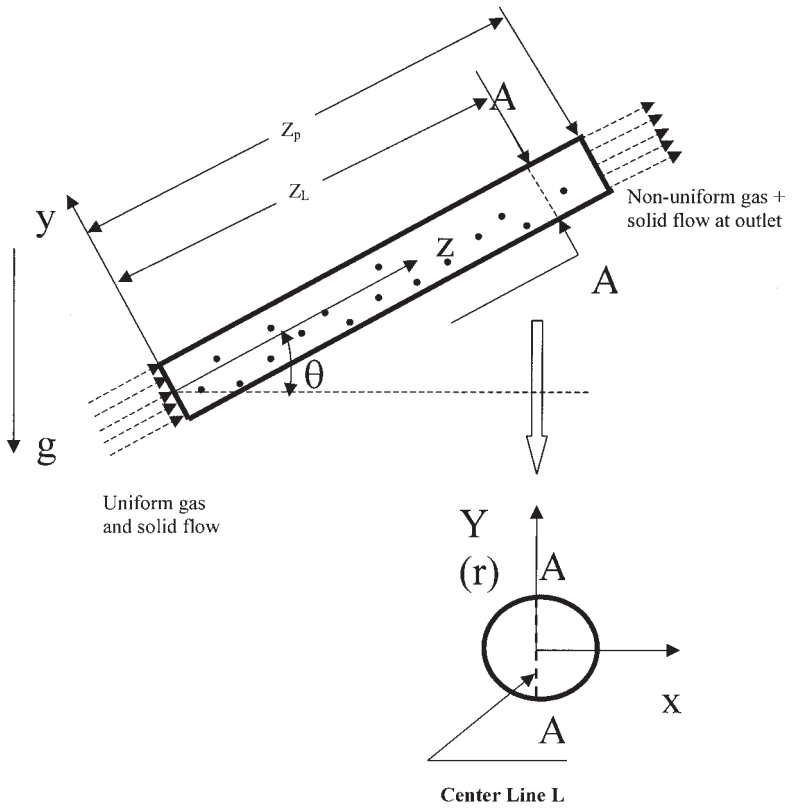

Figure 1. Simulation geometry.

The inclination angle of the conveying pipe varies from 0 to 90°. The diameters of the pipe used in the current studies are 3.05, 4.0, and 8.0 cm. The flow quantities predicted normally taken at the fully developed region along the center line L at the cut section A, Z_L meters away from the feeding end. The length of the conveying pipe is Z_P.

probed by grid schemes c (400 × 10 × 10) and d (800 × 12 × 12). The pressure gradient calculated between 7.5 and 8.5 m away from the feeding end of the conveying pipe was found to decrease with the grid becoming finer until the grid size reached 400 × 10 × 10 (grid scheme c).

Figure 2(ii) shows the effects of grid size on the solids volume fraction distribution over the $x = 0$ plane at 7.5 m away from the feeding point of the conveying tube. The simulation using a coarse grid scheme (grid scheme a: 200 × 6 × 6) averaged out the axial nonuniformity in solids volume fraction distribution, whereas the finer grid scheme predicted the axial nonuniformity in the solids volume fraction. This is in agreement with the finding of Agrawal et al. (2001) and Zhang and VanderHeyden (2001). From Figures 2(i) and (ii), we may conclude that flow features are almost grid-independent when the grid size reaches 400 × 10 × 10 (grid scheme c).

Comparison with Tsuji and Morikawa (1982)

Using a laser-Doppler anemometer, Tsuji and Morikawa (1982) measured the mean gas-phase velocity profiles, mean solids-phase velocity profiles, and gas-phase velocity fluctuations in a horizontal pipe (diameter = 30.5 mm) at 3.56 m away from the solids feeding end. In their experiments, polystyrene particles (density = 1020 kg/m^3; diameter = 200 μm) were used.

Table 1. Model Constants Appearing in κ–ε Equations (Eqs. A11–A14)

$C_{1\varepsilon}$	$C_{2\varepsilon}$	C_μ	σ_k	σ_ε
1.44	1.92	0.09	1.0	1.3

To compare numerical results with experimental measurements, simulations are carried out using the geometry shown in Figure 1 with $\theta = 0°$ and $Z_L = 3.56$ m. Louge et al. (1991) and Bolio et al. (1995) numerically investigated gas-solid flows in a vertical conveying pipe using the same type of particles (polystyrene) and conveying pipe material. Because the restitution coefficients of particle–particle collisions and particle–wall collisions depend mostly on the material properties of particles and wall, the same restitution coefficients for particle–particle collisions and particle–wall collisions as those used by Louge et al. (1991) and Bolio et al. (1995), that is, $e_s = 0.9$ and $e_w = 0.7$ were used in this study. The specularity factor is related to overall wall roughness and may also depend on the orientation of the conveying tube in addition to the material properties of the pipe and particles. Because there is no other experimental value available in the literature, the specularity factor is specified as $\phi = 0.002$, as adopted by Bolio et al. (1995). This specularity factor means that only 0.2% of tangential momentum is lost after particles collide with the wall. This loss of tangential momentum is quite reasonable for a smooth glass pipe used in experiments by Tsuji and Morikawa (1982). Model constants for κ–ε closures are shown in Table 1.

Figure 3 shows the comparison of numerical predictions

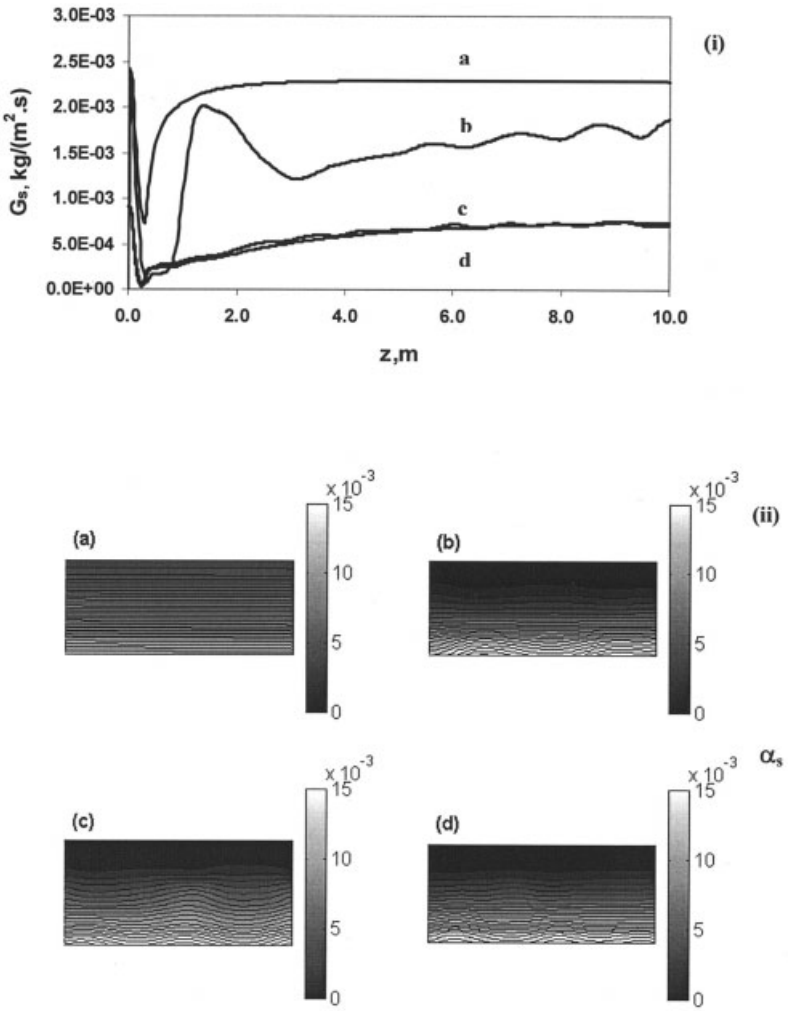

Figure 2. Effects of the grid scheme in the pneumatic conveying of 2.8-mm particles in a pipe (diameter = 4 cm).

(i) Solids mass flux evaluated at the central control volumes along the z-axis; (ii) Solid fraction (α_s) distribution: (a) 200 × 6 × 6; (b) 300 × 8 × 8; (c) 400 × 10 × 10; (d) 800 × 12 × 12. U = 15.6 m/s, G_s = 49.7 kg/(m^2·s). e_s = 0.9, e_w = 0.7, ϕ = 0.002. (θ, Z_P) = (0°, 10 m).

using models with/without considering gas-phase turbulence at superficial velocity U = 10 m/s and solids mass loading m = 3.3. It has been found that the model including gas-phase turbulence gave much better predictions. Figure 4a shows the comparison between numerical predictions and experimental measurements for the mean velocity profiles of the gas phase at various solids mass loadings with U = 15 m/s. The numerical results agree reasonably well with the measurements by Tsuji and Morikawa (1982). Experimental data demonstrated that the mean gas velocity profiles exhibited a local minimum (marked by point Q in Figure 4a) near the pipe center with increasing solids mass loadings, although no explanation was given for this phenomenon. Similar measurements were carried out by Kussin and Sommerfeld (2001) using PDA in a horizontal channel with particles of diameter 0.625 mm at solids mass loading m = 1.95 and gas-phase velocity U = 18.5 m/s. However, no local minimum in the gas-phase velocity profile was found, as with the findings of the present study.

Figure 4b shows the comparison between numerical predictions and experimental measurements for the mean velocity profiles of the solids phase (Tsuji and Morikawa, 1982) at various solids mass loadings under a constant air superficial velocity U = 15 m/s. It can be seen that the model predictions agree quite well with the experimental measurements at the lower portion of the conveying tube, whereas underpredictions are found at the upper portion of the conveying tube. This could be a result of lateral particle size segregations attributed to gravity. In the experiments by Tsuji and Morikawa (1982), the particles used were polydispersed and therefore exhibited size-dependent migration, whereas such behavior is absent in the present calculation because the particles are assumed to be monodispersed. In the horizontal pneumatic conveying of solids, larger particles move along the bottom section of the conveying tube with lower velocities and smaller particles move along the upper section of the conveying tube with higher velocities. This could result in the deviation observed between the model predictions and experimental measurements.

In the current work, the numerical model seems to overpredict the gas-phase turbulence intensities. Figure 4c shows one comparison of the axial gas-phase velocity fluctuation intensity obtained experimentally with that from the present model. Several factors may contribute to the deviation from experi-

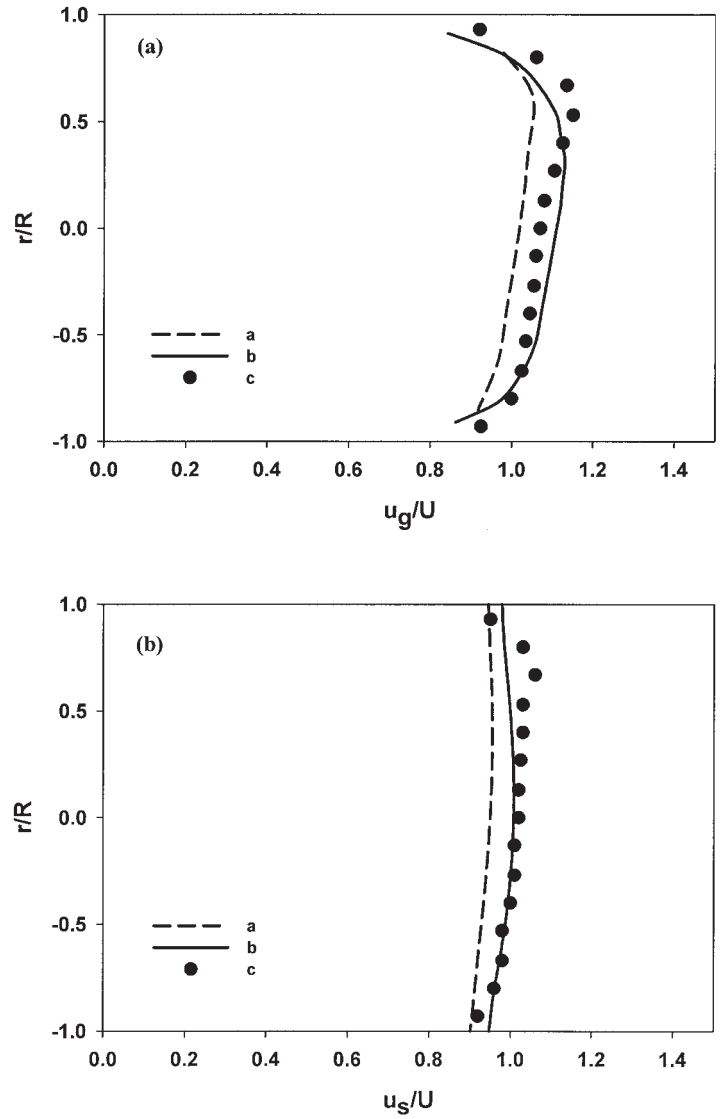

Figure 3. Comparison of the model predictions with the measurements by Tsuji and Morikawa (1982) of pneumatic conveying of 200-μm solids in a pipe with a diameter of 3.05 cm.

(a): u_g/U; (b): u_s/U; along line L at $U = 10$ m/s; $m = 2.2$, $(\theta, Z_L, Z_P) = (0°, 3.56$ m, 4 m). a, laminar flow; b gas turbulence; c, measurements by Tsuji and Morikawa (1982).

mental result (especially near the bottom of the pipe). The κ–ε model has its intrinsic deficiency on the isotropic eddy viscosity assumption. Particles used in real experiments were polydispersed and significant lateral movement was introduced as the result of different particle sizes.

Sensitivity analysis of the model parameters

Sensitivity analysis is carried out for the particle–particle and particle–wall collision restitution coefficients for the horizontal conveying of 200-μm particles. The analysis shows that the results are not very sensitive to the particle–particle collision restitution coefficient (e_p from 0.85 to 0.95) under the condition tested (data not shown). Changing the particle–wall restitution coefficient from 0.65 to 0.75 also reveals that e_w has limited effects on the model predictions. This is consistent with the study results obtained by Bolio et al. (1995) in the vertical dilute-phase pneumatic conveying of 200-μm particles.

For large particles (2.8 mm), the horizontal pneumatic conveying results reveal that the particle–wall collision restitution coefficient has a much more significant effect on the particle distribution, whereas the particle–particle restitution coefficient has no significant effect on the qualitative flow features, as shown in Figure 5.

Simulation results also reveal that axial nonuniformity is much more pronounced when particle–wall collisions are more inelastic, that is, smaller e_w (data not shown). Gravity certainly plays a major role in the flow features observed [refer to Figure 2(ii)d]. However, if this is just a gravitational sedimentation effect, the system may not exhibit axial (along the pipe) nonuniformity and a layer pattern of solid distribution should be

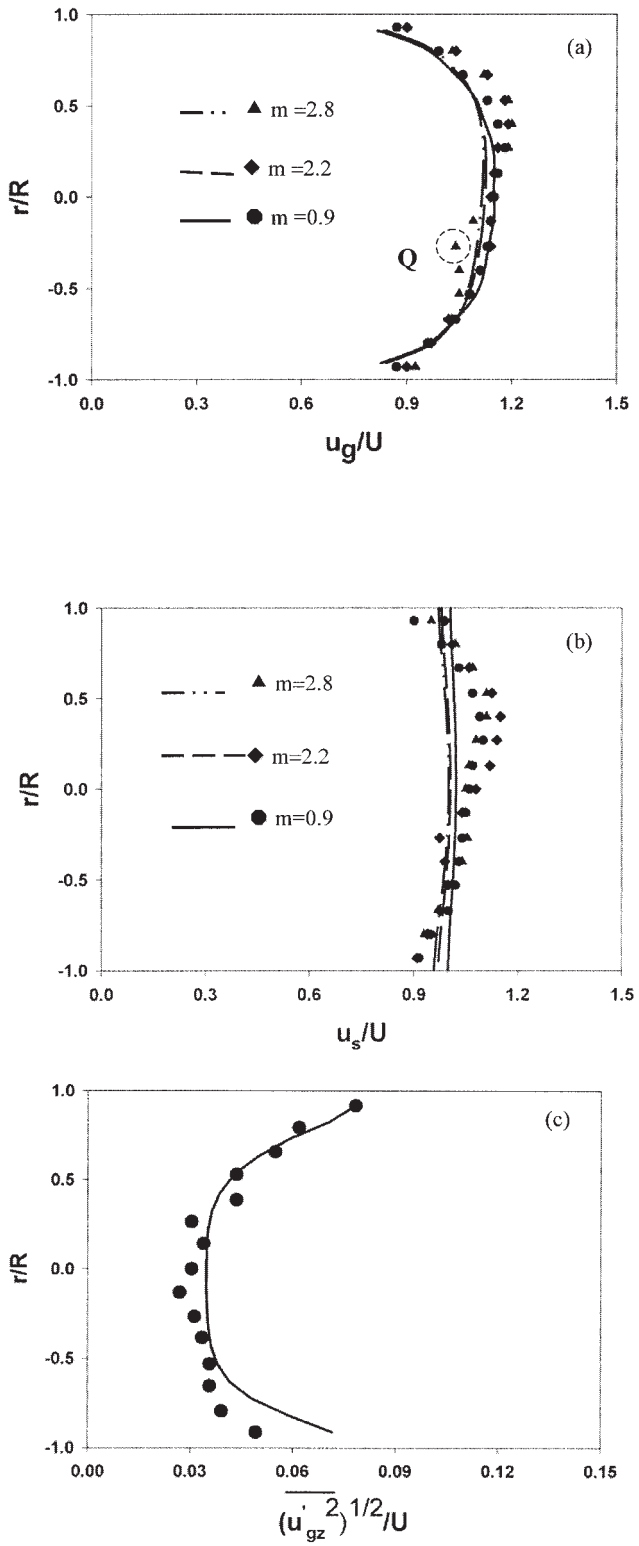

Figure 4. Comparison of the model predictions with the measurements by Tsuji and Morikawa (1982) of pneumatic conveying of 200-μm solids in a pipe with a diameter of 3.05 cm.

(a) u_g/U; (b) u_s/U; (c) $[(\overline{u'_{gz}})^2]^{1/2}/U$ along the line L at $U = 15$ m/s; $m = 2.8$; $(\theta, Z_L, Z_P) = (0°, 3.56$ m, 4 m).

observed. It is seen that the particle–wall collision has a very significant influence on the solid density patterns developed. The solids "cloud" formations are probably attributable to energy dissipation associated with particle random motion by particle inelastic collision or viscous dissipation resulting from the gas phase.

Figure 6 shows the model predictions for three different specularity factors (0.002, 0.01, and 0.02) at $(U, m) = (15$ m/s, 2.8) for 200-μm particles in a horizontal pipe. It is found that the specularity factor has relatively greater effects on the flow quantities. The gas and solids velocities decrease with increasing specularity factor, whereas the solid volume fraction increases with a higher specularity factor. This is because the momentum loss of solids phase increases with higher specularity factor. The shift of the maximum in solids volume fraction profiles toward the center of the conveying pipe is more obvious with increasing specularity factor, which suggests that particle–wall interaction has a substantial influence on the solids distribution in the flow. The variation of solid velocity is around 30% when the specularity factor is varied by one order (from 0.002 to 0.02). Sensitivity analysis results also revealed that the numerical results were found not to be very sensitive to the restitution coefficient of particle–particle collisions for 200-μm particles under the dilute flow condition investigated, which is consistent with the work by Bolio et al. (1995). Similar effects of the specularity factor on the flow features are observed in the 45° inclined tube pneumatic conveying of 3-mm particles.

Influence of inclination angles

Figure 7 shows the solids volume fraction, gas-phase velocity, and solid-phase velocity profiles of 3-mm particles (conveying velocity $U = 17.56$ m/s, solids mass loading $m = 3.85$) under various inclination angles. Figure 7a shows that the solids volume fraction increases with increasing inclination angles and the extent of asymmetric distribution in solids volume fraction decreases with increasing inclination angles. In horizontal conveying, solid particles are more concentrated at the bottom portion of the conveying pipe, as a result of gravitational forces, which is perpendicular to the flow direction. In vertical conveying, in contrast, the distribution of solid particles shows axis-symmetry, given that gravity is aligned parallel to the flow direction.

As stated earlier, gas-phase velocity profiles were mainly affected by the interaction between the two phases, which depends primarily on the solids volume fraction and slip velocity between gas and solids. Henceforth, from the solids volume fraction distributions, it would be no surprise to find that the asymmetry of the gas velocity profile in horizontal conveying is gradually lost with increasing θ until a symmetric velocity profile is obtained in the vertical conveying case (Figure 7b). Figure 7c shows the corresponding solids velocity profiles. The solids velocity in horizontal conveying is the largest and gradually decreases with increasing inclination angles. This is attributed partly to the momentum transfer from the gas phase to the solid particles through interphase interaction, which is used to lift the particles when the inclination angle is not zero.

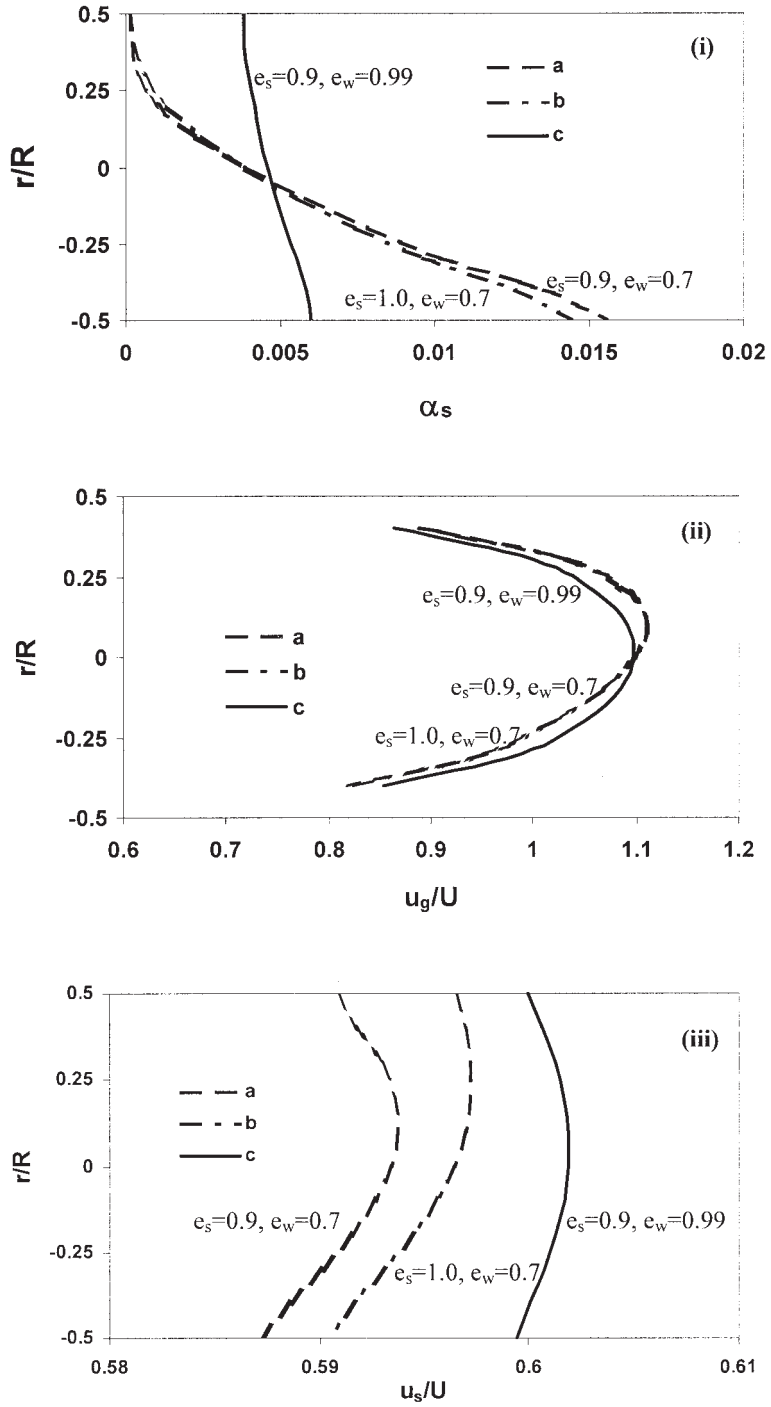

Figure 5. Predictions for distribution of (i) solids volume fraction α_s; (ii) gas velocity u_g, and (iii) solids velocity u_s along line L of the pneumatic conveying of 2.8 mm particles in a pipe with a diameter of 4 cm.

(a) e_s = 0.9, e_w = 0.7; (b) e_s = 1.0, e_w = 0.7; (c) e_s = 0.9, e_w = 0.99. U = 15.6 m/s, G_s = 49.7 kg/(m^2·s), (θ, Z_L, Z_P) = (0°, 7.5 m, 10 m), ϕ = 0.002.

Feeding conditions

Rao et al. (2001) found that feeding characteristics exert significant effects on the flow features. To examine the influence of fluctuations from the feeding end, fluctuations in the conveying airflow rate and solids feeding rate in various forms were introduced in the conveying system and the flow rate and flow behaviors at the downstream side were monitored.

The results presented in Figures 2–7 are steady-state results. After the system has reached a steady state (defined as a flow field whose properties at every point do not change with time),

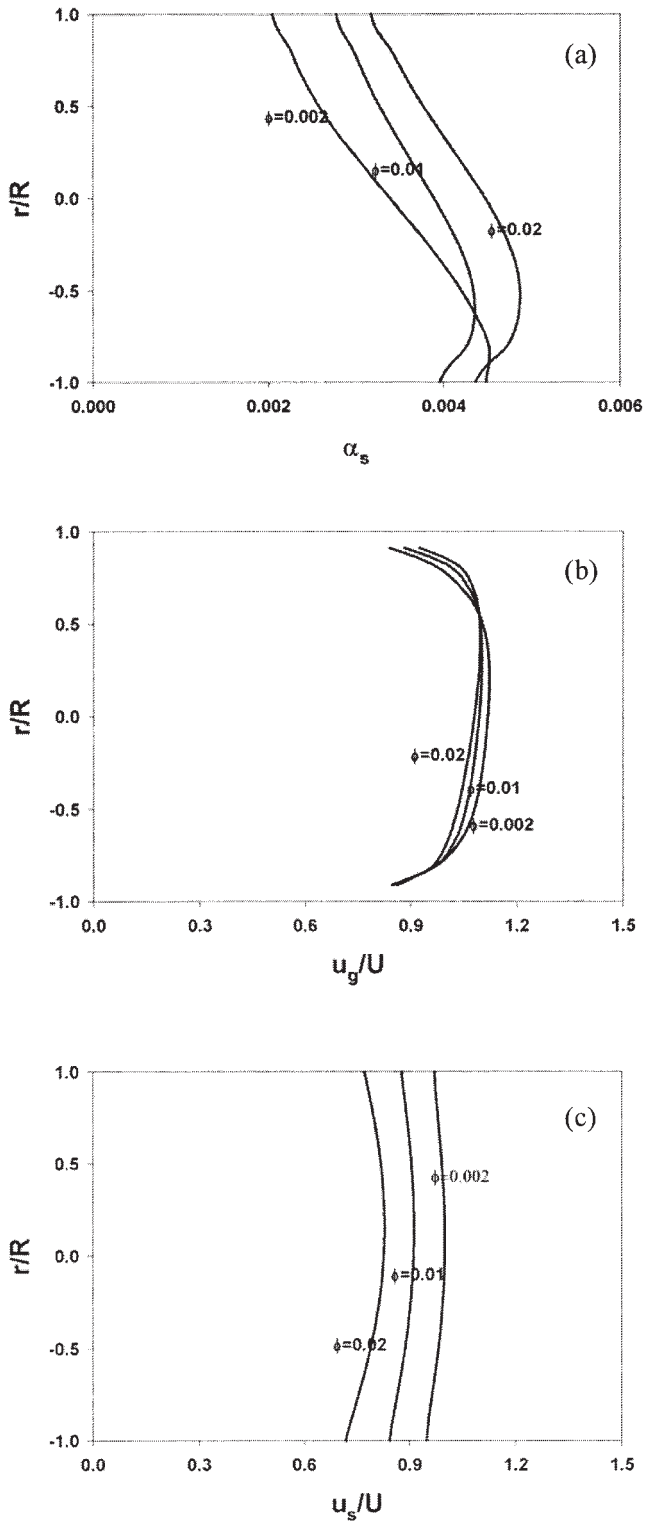

Figure 6. Effect of specularity factor ϕ on flow variable profiles along line L in the pneumatic conveying of 200-μm particles through a pipe with a diameter of 3.05 cm.

(a) α_s; (b) u_s/U; and (c) u_g/U. U = 15 m/s, m = 2.8; e_s = 0.9, e_w = 0.7; (θ, Z_L, Z_P) = (0°, 3.56 m, 4 m).

a sinusoidal fluctuation with a frequency of 3.3 Hz and amplitude equal to 10% of the averaged air velocity was introduced at the entrance of the system. Figure 8 shows the contour plots of the time evolution of solids volume fraction distribution after introducing the fluctuation of airflow rate at the entrance. It can be clearly seen that the solids nonuniformities move along the conveying pipe with time. The corresponding pressure detected at the downstream side (7.5 m) experienced fluctuations of the same frequency, with amplitude around 40% of the time-averaged pressure detected at that location.

Three different types of perturbations (one- and two-step perturbations and sinusoidal fluctuations in the solids volume fraction at the feeding point with frequency 3.3 Hz and amplitude equal to 10 and 50% of the mean solids volume fraction) were introduced into the system with a steady initial flow field. To probe the influence of the solids volume fraction at the feeding end, the flow quantities were monitored along the conveying pipe to explore the propagation of the fluctuations.

One-step (period = 0.25 s) and two-step (period = 0.25 s; interval = 0.25 s) perturbations with amplitude 50% (based on quantities at the inlet) of the averaged solids volume fraction were introduced at the entrance. Figures 9a and 9b show the solids volume fraction profiles detected at the central control volume obtained along the conveying line of one- and two-step perturbations, respectively. The introduced step perturbations were dispersed axially, which resulted in the height of the pulse becoming lower and the width being larger, as shown in Figure 9a. The variances associated with these four different axial positions are 0.0090, 0.0171, 0.0102, and 0.0101, respectively. For the case of two-step perturbations, the two pulses eventually joined together while marching along the tube as a result of axial dispersion. Qualitatively similar results were found for the case of step perturbations with amplitude about 10% of the averaged solids volume fraction at the entrance. However, the axial dispersion of the fluctuations for the 10% perturbation was much faster than that for the 50% perturbation.

The solids volume fractions were monitored at the downstream side of the conveying pipe after introducing 10 and 50% sinusoidal fluctuations in the solids volume fraction (referring to the inlet average quantity) at the feeding point. For both cases, the fluctuations detected at the downstream side have fluctuation intensities smaller than the perturbation introduced. To characterize the propagation of the fluctuations, power spectra of the fluctuation along the conveying tube were analyzed. Figure 10a shows the power spectra of the solids volume fraction fluctuations obtained at the central control volume located at 1.0, 3.3, 6.0, and 8.5 m away from the feeding end of the conveying pipe for 10% fluctuations. It can be observed that the dominant frequency in solids volume fraction fluctuation shifted from 3 Hz toward a lower frequency along the conveying tube. Figure 10b shows the power spectra of the solids volume fraction detected at the central control volume located at 1.0, 3.3, 6.0, and 8.5 m away from the feeding point along the conveying tube for 50% fluctuations. It is observed that the fluctuation of solids volume fraction has the same frequency as the perturbation introduced.

Studies of step fluctuations showed that slower axial dispersion was observed for 50% fluctuations compared to 10% fluctuations in the solid feeding at the entrance. This is consistent with the result of the investigation on sinusoidal fluctuations. After introducing sinusoidal fluctuations with a fre-

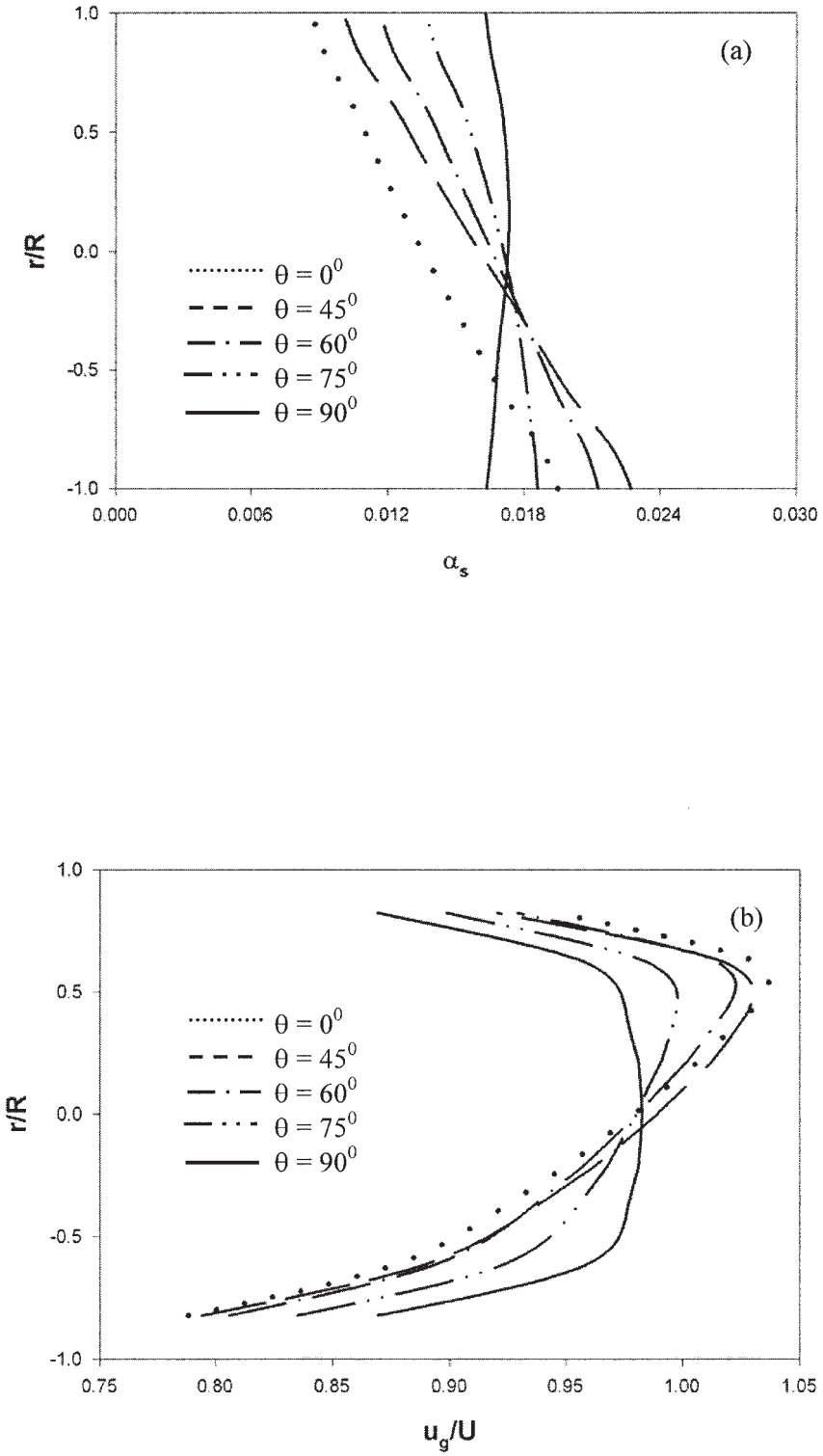

Figure 7. Influence of inclination angle on the flow quantities along line L of pneumatic conveying of 3.0-mm particles in a pipe with a diameter of 8.0 cm.

(a) α_s; (b) u_g/U; (c) u_s/U. $m = 3.85$; $e_s = 0.9$, $e_w = 0.7$, $\phi = 0.02$; $(Z_L, Z_P) = (7.5\text{ m}, 10\text{ m})$.

quency of 3.3 Hz in the solids feeding, a 3.3-Hz density wave was found to prevail through the conveying line for 50% fluctuations, whereas the characteristic frequency of the density wave was reduced along the conveying line for 10% fluctuations.

According to Agrawal et al. (2001) and Wylie and Koch (2000), dissipation of pseudothermal energy arising from particle–particle inelastic collisions and as a result of gas-phase viscous force tend to enhance particle cluster formation. There-

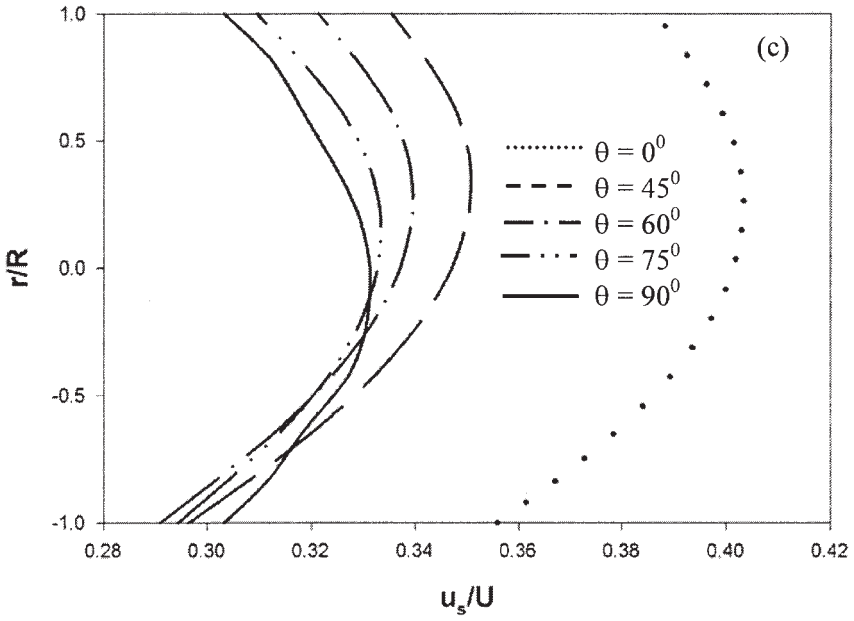

Figure 7. Continued

fore the generation of pseudothermal energy would be the mechanism for the dispersion of the solids clusters. The pseudothermal energy, as shown in Eq. A24 of the Appendix, is generated by the work of shear stresses and interfacial flux of kinetic energy from gas-phase turbulence, dissipated as the result of inelastic particle–particle collisions and gas-phase viscous force. Hence, gas-phase turbulence and shear stresses in the solids phase might be the main causes for axial dispersion of solids clouds. In contrast, particle–particle inelastic collisions and gas-phase viscous dissipation seem to be the

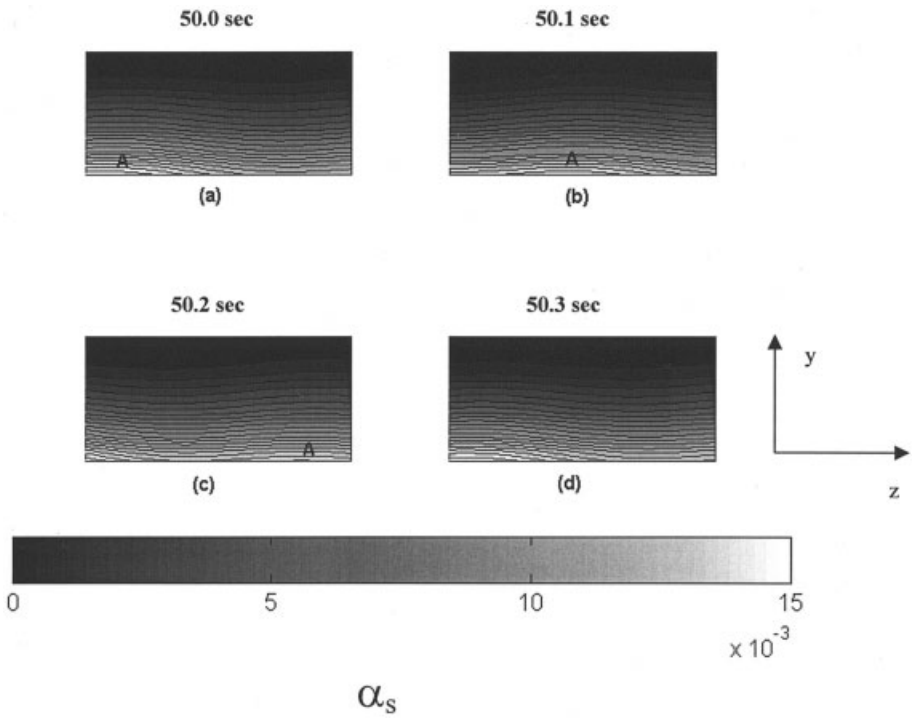

Figure 8. Contour plots of instantaneous solids volume fraction (α_s) distribution over the central vertical plane between 7.5 and 10 m away from the feeding end of the pneumatic conveying of 2.8-mm particles in a pipe with a diameter of 4.0 cm.

(a) −50.0 s; (b) −50.1 s; (c) −50.2 s; (d) −50.3 s. U = 15.6 m/s, G_s = 49.7 kg/(m^2·s); e_s = 0.9, e_w = 0.7, ϕ = 0.002. The marked tracer point is shown as point A. This point is no longer visible in panel (d). (θ, Z_P) = (0°, 10 m).

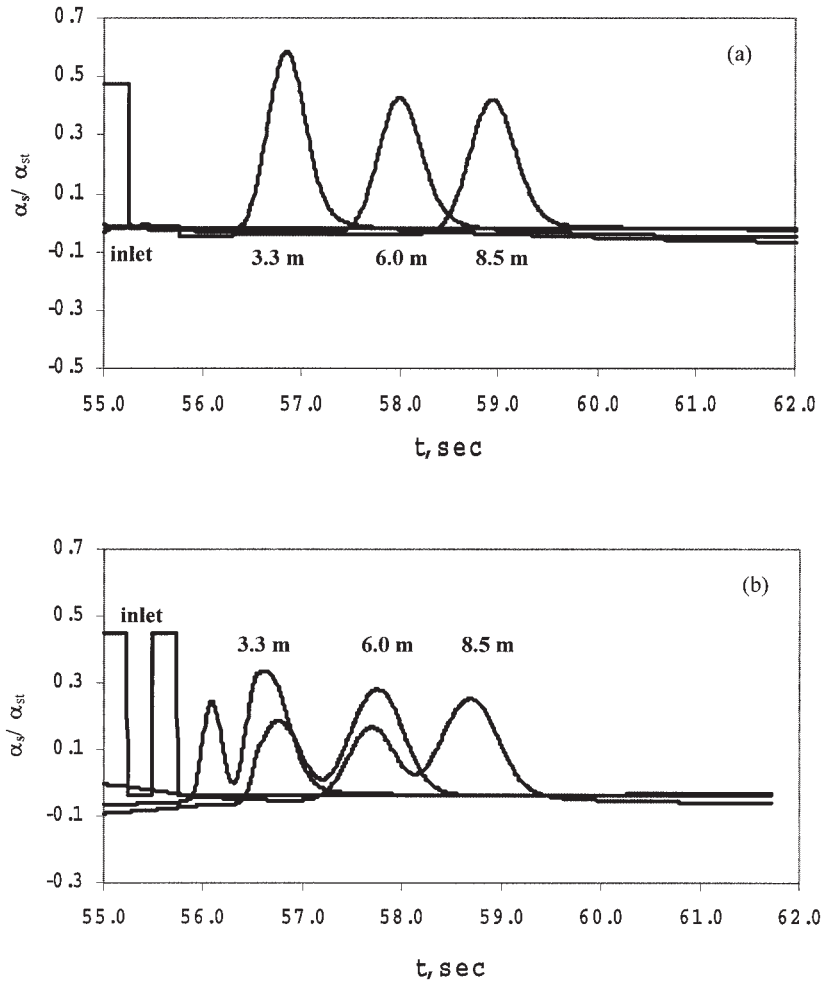

Figure 9. Time evolution of solids volume fraction detected at the central control volume of the cross section along the *z*-axis of the pneumatic conveying of 2.8-mm particles in a pipe with a diameter of 4.0 cm.

The fluctuations in solids volume fraction (50%) are introduced at the entrance: (a) one-step perturbation introduced; (b) successive two-step perturbation introduced at the entrance. U = 15.6 m/s, G_s = 49.7 kg/(m^2·s); e_s = 0.9, e_w = 0.7, ϕ = 0.002; (θ, Z_P) = (0°, 10 m).

main mechanisms for enhancing solids clouding. Compared to the 10% fluctuations, the concentrations in the solids clouds for 50% fluctuations are higher. Therefore, particles in the solid cloud undergo more frequent collisions and viscous dissipation (which depends on local solids volume fraction) is also larger. This may provide an explanation for the reduction of axial dispersion for the 50% fluctuations.

To investigate the effects of random fluctuations in solids flow rate on flow features, a test simulation was carried out after introducing a random signal, as shown in Figure 11a (generated using the random function in MatLab software). Solids volume fractions were detected along the conveying line (Figure 11b). It was observed that the density waves became weaker along the conveying pipe, which is probably attributable to particle axial dispersion. This observation is consistent with the step fluctuation simulation results but with much more complicated flow structures.

Conclusions

In this work, 3-D CFD simulations were carried out to examine the turbulent pneumatic conveying of granular solids through horizontal, inclined, and vertical pipes. Model evaluation was first performed using the experimental data of Tsuji and Morikawa (1982) in terms of the gas- and solid-phase mean velocities, as well as the axial turbulence intensity. Sensitivity analysis of predictions on the model parameters was presented. Effects of inclination angle and feeding condition on the flow quantities were also investigated. Conclusions based on the present work are presented in the following point form:

(1) The model was able to capture the basic flow features of pneumatic conveying systems. The numerical model incorporating gas-phase turbulence gave much better results, which confirmed that gas-phase turbulence plays a key role in dilute pneumatic conveying of solids.

(2) The asymmetries in the mean flow quantities (gas velocity, solids velocity, and solid volume fraction) are predicted. These are consistent with earlier experimental results (Kussin and Sommerfeld, 2001; Tsuji and Morikawa, 1982).

(3) Sensitivity analysis revealed that the specularity factor had a significant effect on the model predictions. Particle–wall collision had a more significant effect on the flow features for large particles (3 mm) than for smaller particles (0.2 mm).

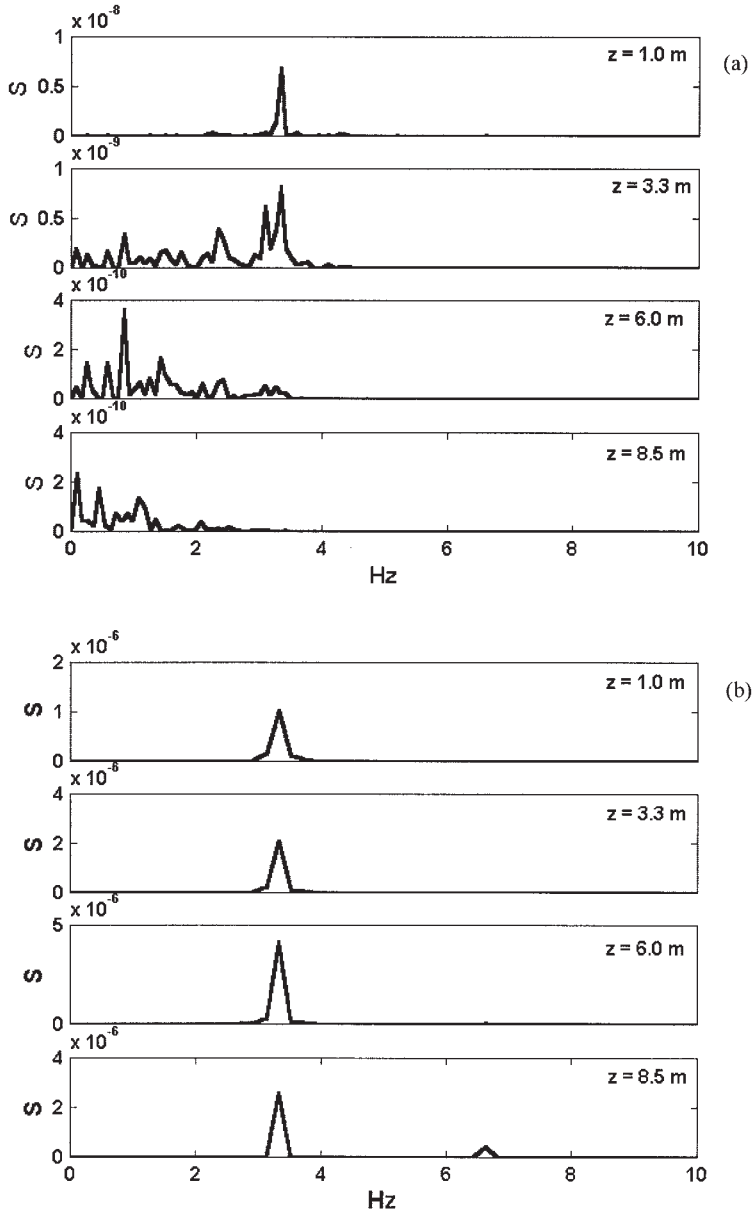

Figure 10. Power spectrum of solid volume fraction fluctuations of pneumatic conveying of 2.8-mm particles in a pipe with a diameter of 4.0 cm.

The fluctuations in solids volume fraction are introduced at the feeding point of the conveying pipe with frequency 3.3 Hz and (a) amplitude 10% of the mean value; (b) amplitude 50% of the mean value. $U = 15.6$ m/s; $G_s = 49.7$ kg/(m^2·s); $e_s = 0.9$, $e_w = 0.7$, $\phi = 0.002$; $(\theta, Z_P) = (0°, 10$ m).

Large particles had larger slip velocity and asymmetric distribution in the horizontal conveying line.

(4) Results on various fluctuations at the feeding end revealed that solid particles experienced axial dispersion along the conveying pipe. The results supported the argument that larger fluctuations in solids feeding rate associated with the rotary valve might be the mechanism responsible for density waves in the homogeneous flow regime observed in the experimental works of Rao et al. (2001) and Zhu et al. (2003).

(5) The model seems to overpredict axial turbulence intensity. Several factors may contribute to the deviation from experimental results. (i) The κ–ε model has an intrinsic deficiency because of its isotropic eddy viscosity assumption. (ii) Particles were assumed monodispersed in the current work, whereas in reality the particles used were polydispersed. (iii) The closure for fluctuation velocity correlation is based on an empirical formula. Derivation of new closure for this term, starting from first principles, may be of interest to researchers in the future.

Notation

C_D = drag coefficient, dimensionless
d_s = particle diameter, m
e_s = restitution coefficient of particle–particle collision, dimensionless

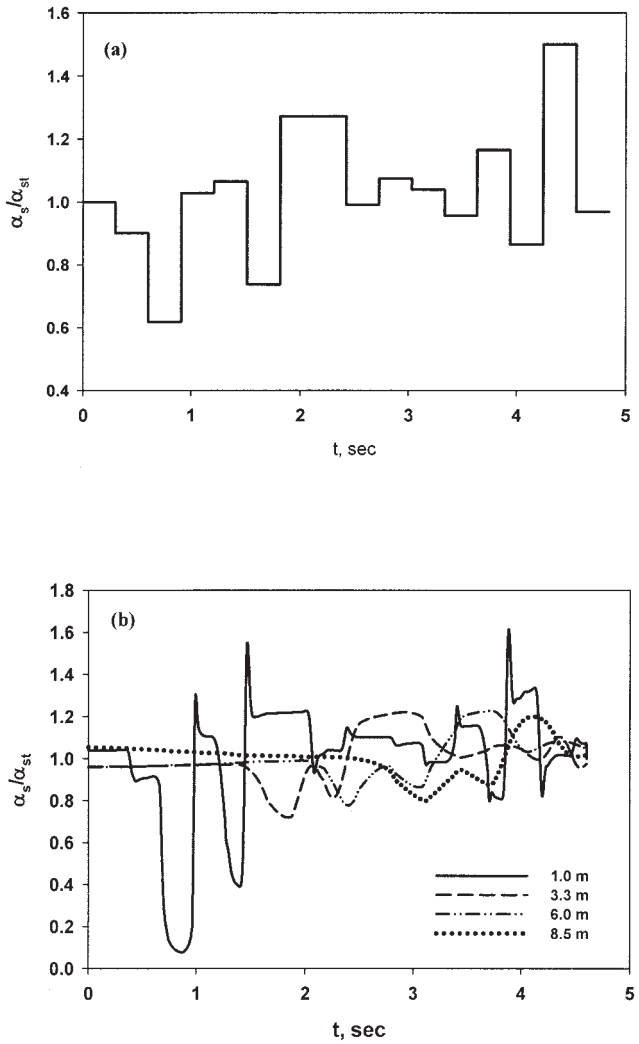

Figure 11. Solid volume fractions detected along the conveying line after introducing random fluctuations with 3.3 Hz and 50% maximum amplitude of the average solids volume fraction at the feeding end.

Pneumatic conveying of 2.8-mm particles in a pipe with a diameter of 4 cm. $U = 15.6$ m/s, $G_s = 49.7$ kg/(m^2·s); $e_s = 0.9$, $e_w = 0.7$, $\phi = 0.002$; $(\theta, Z_P) = (0°, 10$ m).

e_w = restitution coefficient of particle–wall collision, dimensionless
$\vec{g}$ = gravity, m/s^2
g_0 = radial distribution function, dimensionless
m = solids mass loading, dimensionless
T_s = particle relaxation time, s
p_g = gas-phase pressure, N/m^2
p_s = solids-phase pressure, N/m^2
R = pipe radius, m
Re_s = relative Reynolds number, dimensionless
$\bar{\bar{S}}$ = deformation tensor, s^{-1}
$S_{\kappa 1,\, S\kappa 2}$ = source term in the turbulence model (κ equation), kg/(m·s^3)
$S_{\varepsilon 1,\, S\varepsilon 2}$ = source term in the turbulence model (ε equation), kg/(m·s^4)
$\vec{u}_g$ = gas-phase velocity, m/s
$\vec{u}_g'$, $\vec{u}_s'$ = fluctuation velocity of gas and solids phases, m/s
$\vec{u}_s$ = solid-phase velocity, m/s
u_{gz} = z-component of gas-phase velocity, m/s
U = superficial gas velocity, m/s

Greek letters

α_g = volume fraction of gas phase, dimensionless
α_s = volume fraction of solid phase, dimensionless
$\alpha_{s,max}$ = random close packing solids volume fraction, dimensionless
γ = dissipation rate of granular energy, kg/(m·s^3)
ε = dissipation rate of turbulence kinetic energy, m^2/s^3
Θ_s = granular temperature, m^2/s^2
κ = gas-phase turbulence kinetic energy per unit mass, m^2/s^2
κ_s = solids thermal conductivity, kg/(m·s)
μ_b = bulk viscosity of gas phase, kg/(m·s)
$\mu_{\mathrm{eff},g}$ = effective viscosity of gas phase, kg/(m·s)
μ_g = viscosity of gas phase, kg/(m·s)
μ_s = viscosity of solid phase, kg/(m·s)
$\mu_{s,col}$ = collisional contribution to the solid-phase viscosity, kg/(m·s)
$\mu_{s,\mathrm{kin}}$ = kinetic contribution to the solid-phase viscosity, kg/(m·s)
μ_t = gas-phase turbulence viscosity, kg/(m·s)
ρ_g = density of air, kg/m^3
ρ_s = density of solids particles, kg/m^3
$\bar{\bar{\tau}}_s$ = stress tensor of solid phase, kg/(m·s^2)
$\bar{\bar{\tau}}_g$ = stress tensor of gas phase, kg/(m·s^2)
$\bar{\bar{\tau}}_{s,w}$ = stress tensor of solid phase at the wall, kg/(m·s^2)
φ_{sg} = dissipation rate of granular energy arising from gas solids interaction, kg/(m·s^3)
ϕ = specularity factor of solid-phase, dimensionless

Subscripts

g = gas phase
s = solids phase
w = wall

Acknowledgments

We acknowledge the National University of Singapore for financial support under Grant R279-000-095-112. We also thank Professor Sankaran Sundaresan for many helpful discussions on the project and Wee Chuan Lim for technical support on the preparation of this manuscript.

Literature Cited

Agrawal, K., P. N. Loezos, M. Syamlal, and S. Sundaresan, "The Role of Mesoscale Structures in Gas-Solid Flows," *J Fluid Mech.*, **445**, 151 (2001).

Anderson, T. B., and R. Jackson, "A Fluid Mechanical Description of Fluidized Beds," *Ind. Eng. Chem. Fundam.*, **6**, 527 (1967).

Bolio, E. J., J. A. Yasuna, and J. L. Sinclair, "Dilute Turbulent Gas-Solid Flow in Risers with Particle–Particle Interactions," *AIChE J.*, **41**, 1375 (1995).

Coelho, P., and J. C. F. Pereira, "Calculation Procedure for 3-D Laminar Flows in Complex Geometries Using a Nonstaggered Nonorthogonal Grid System," *Appl. Math. Modelling*, **17**, 562 (1993).

Ding, J., and D. Gidaspow, "A Bubbling Fluidization Model Using Kinetic Theory of Granular Flow," *AIChE J.*, **36**, 523 (1990).

Gidaspow, D., *Multiphase Flow and Fluidization: Continuum and Kinetic Theory Description*, Academic Press, Boston, MA (1994).

Hirota, M., Y. Sogo, T. Marutani, and M. Suzuki, "Effect of Mechanical Properties of Powder on Pneumatic Conveying in Inclined Pipe," *Powder Technol.*, **122**, 150 (2002).

Huber, N., and M. Sommerfeld, "Characterization of the Cross-Sectional Particle Concentration Distribution in Pneumatic Conveying Systems," *Powder Technol.*, **79**, 191 (1994).

Johnson, P. C., and R. Jackson, "Frictional–Collisional Constitutive Relations for Granular Materials, with Application to Plane Shearing," *J. Fluid Mech.*, **176**, 67 (1987).

Kenning, V. M., and C. T. Crowe, "On the Effect of Particles on Carrier Phase Turbulence in Gas-Particle Flows," *Int. J. Multiphase Flow*, **23**, 403 (1997).

Kussin, J., and M. Sommerfeld, "Investigation of Particle Behavior and Turbulence Modification in Particle Laden Channel Flow," *Proceedings of PARTEC '2001*, Nuremberg, Germany (2001).

Launder, B. E., and D. B. Spalding, "The Numerical Computation of Turbulence Flows," *Comput. Method Appl. M.*, **3**, 269 (1974).

Levy, A., T. Mooney, P. Marjanovic, and D. J. Mason, "A Comparison of Analytical and Numerical Models with Experimental Data for Gas-Solid Flow through a Straight Pipe at Different Inclinations," *Powder Technol.*, **93**, 253 (1997).
Lien, F. S., W. L. Chen, and M. A. Leschziner, "A Multiblock Implementation of a Non-Orthogonal, Collocated Finite Volume Algorithm for Complex Turbulent Flows," *Int. J. Numer. Methods Fluids.*, **23**, 567 (1996).
Louge, M., E. Mastorakos, and J. Jenkins, "The Role of Particle Collisions in Pneumatic Transport," *J. Fluid Mech.*, **231**, 345 (1991).
Lun, C. K. K., and H. S. Liu, "Numerical Simulation of Dilute Turbulent Gas-Solid Flows in Horizontal Channels," *Int. J. Multiphase Flow*, **23**, 575 (1997).
Lun, C. K. K., S. B. Savage, D. J. Jeffrey, and N. Chepurnity, "Kinetic Theories for Granular Flow: Inelastic Particles in Couette Flow and Slightly Inelastic Particles in a General Flow Field," *J Fluid Mech.*, **140**, 223 (1984).
Mallo, A. M., "Heat Transfer Rate Predictions in Dilute and Dense Gas-Solid Flow," PhD Thesis, Carnegie Mellon University, Pittsburgh, PA (1997).
Ocone, R., S. Sundaresan, and R. Jackson, "Gas-Particle Flow in a Duct of Arbitrary Inclination with Particle–Particle Interactions," *AIChE J.*, **39**, 1261 (1993).
Owen, P. R., "Pneumatic Transport," *J. Fluid Mech.*, **39**, 407 (1969).
Patankar, S. V. *Numerical Heat Transfer and Fluid Flow*, Hemisphere Publishing, Washington, DC (1980).
Peirano, E., and B. Leckner, "Fundamentals of Turbulent Gas-Solid Flows Applied to Circulating Fluidized Bed Combustion," *Prog. Energy Combust. Sci.*, **24**, 259 (1998).
Peirano, E., V. Delloume, F. Johnsson, B. Leckner, and O. Simonin, "Numerical Simulation of the Fluid Dynamics of a Freely Bubbling Fluidized Bed: Influence of the Air Supply System," *Powder Technol.*, **122**, 69 (2002).
Rao, S. M., K. W. Zhu, C. H. Wang, and S. Sundaresan, "Electrical Capacitance Tomography Measurements on the Pneumatic Conveying of Solids," *Ind. Eng. Chem. Res.*, **40**, 4216 (2001).
Sato, Y., U. Fukuichi, and K. Hishida, "Effect of Inter-Particle Spacing on Turbulence Modulation by Lagrangian PIV," *Int. J. Heat Fluid Flow*, **21**, 554 (2000).
Schuh, M. J., C. A. Schuler, and J. A. C. Humphery, "Numerical Calculation of Particle-Laden Gas Flows Past Tubes," *AIChE J.*, **35**, 466 (1989).
Sinclair, J. L., and R. Jackson, "Gas-Particle Flow in a Vertical Pipe with Particle–Particle Interactions," *AIChE J.*, **35**, 1473 (1989).
Tsuji, Y., and Y. Morikawa, "LDV Measurements of Air-Solid Two-Phase Flow in a Horizontal Pipe," *J. Fluid Mech.*, **120**, 385 (1982).
Wylie, J. J., and D. L. Koch, "Particle Clustering due to Hydrodynamic Interactions," *Phys. Fluids*, **12**, 964 (2000).
Yuan, Z., and E. Michaelides, "Turbulence Modulation in Particulate Flows—A Theoretical Approach," *Int. J. Multiphase Flow*, **18**, 779 (1992).
Zhang, D. E., and W. B. VanderHeydan, "High-Resolution Three-Dimensional Numerical Simulation of a Circulating Fluidized Bed," *Powder Technol.*, **116**, 133 (2001).
Zhang, Y., and J. M. Reese, "The Drag Force in Two-Fluid Models for Gas-Solid Flows," *Chem. Eng. Sci.*, **58**, 1641 (2003).
Zhu, K., S. M. Rao, C. H. Wang, and S. Sundaresan, "Electrical Capacitance Tomography Measurements on the Vertical and Inclined Pneumatic Conveying of Granular Solids," *Chem. Eng. Sci.*, **58**, 4225 (2003).

Appendix: Model Equations

Model equations and boundary conditions used in the present study are summarized as follows. Equations A1 to A4 are the continuity and momentum balance equations for gas and particle phases. Here ρ_g and ρ_s are the gas and particle densities, respectively; $\vec{u}_g$ and $\vec{u}_s$ are the local-averaged gas- and solid-phase velocities, respectively; p_g and p_s are the locally averaged gas- and solid-phase pressures, respectively; $\overline{\overline{\tau}}_g$ is the gas-phase stress and $\overline{\overline{\tau}}_s$, the solid-phase stress; $\vec{g}$ is the gravitational acceleration; β denotes the interphase transport coefficient. In all variables, the subscripts g and s refer to the gas and solid phases, respectively. The volume fractions of gas phase (α_g) and solid phase (α_s) are summed up to unity (Eq. A5).

There are several formulas available for the interphase transport coefficient between the gas and solids phases. Zhang and Reese (2003) developed a new expression for the interphase transport coefficient accounting for relative random motion of particles. In this work, the interphase transport coefficient is evaluated using the empirical formula proposed by Schuh et al. (1989), as shown in Eq. A6, which is applicable to a relatively dilute flow system.

The gas phase is modeled as an isothermal, incompressible Newtonian fluid with the gas-phase viscous stress given by Eqs. A7 and A8. The influence of particles on the effective gas-phase viscosity (Eq. A9) is expressed as that described in Ocone et al. (1993). Turbulent viscosity is determined using Eq. A10, in which κ and ε are the turbulence kinetic energy and turbulence kinetic energy dissipation rate, respectively. The turbulence kinetic energy (κ) and turbulence kinetic energy dissipation rate (ε) are obtained through solving the conservation equations shown in Eq. A11. The source term S_{Y1} (Eq. A12) takes the form proposed by Lauder and Spalding (1974), and the source term S_{Y2} stands for the interactions between the gas- and solid-phase turbulence fluctuations. The correlation between gas and solid fluctuation velocities is modeled by an empirical formula (Eq. A13), as suggested by Mallo (1997).

The stress of the solids phase is given by Eqs. A15–A18. Stress in the solids phase is then transmitted through translation of particles between adjacent layers and collisions between particles. Based on the grain kinetic theory (Bolio et al., 1995; Ding and Gidaspow, 1990; Gidaspow, 1994; Johnson and Jackson, 1987; Johnson et al., 1990; Louge et al., 1991; Ocone et al., 1993; Sinclair and Jackson, 1989), the collisoinal and kinetic viscosities are modeled as Eqs. A19 and A20, respectively. The granular temperature Θ_s can be determined by the conservation equation for pseudothermal energy, as shown in Eq. A24, where k_s (Eq. A26) is the solid-phase conductivity coefficient of pseudothermal energy; γ_s (Eq. A27) is the pseudothermal energy dissipation rate resulting from particle inelastic collisions; and φ_{sg} (Eq. A28) is the pseudothermal energy dissipation or generation rate arising from the interaction between gas and solids phases, as suggested by Mallo (1997).

Proper boundary and initial conditions are needed to solve the coupled nonlinear differential equations. At the inlet, a uniform normal velocity distribution is specified for the gas phase. For the solid phase, uniform distributions in normal velocity, solid granular temperature, and solid volume fraction are provided. Turbulence intensity (the ratio of fluctuation velocity u' to the gas superficial velocity U, $i = u'/U$) and turbulence length scale (l: defined as the size of large energy-containing eddies in the turbulent flows) are given at the inlet for the gas phase. At the outlet, the gas-phase pressure is ambient and all other variables are subjected to the Newmann boundary conditions (that is, $\partial\Phi/\partial z$, *where* Φ refers to flow variables). At the wall the standard wall functions are specified for the gas phase (Lauder and Spalding, 1974). Partial slip boundary conditions for particle–wall interactions (Eqs. A29 and A30), proposed by Johnson and Jackson (1987), are applied in the present study, where ϕ is the specularity factor representing tangential momentum loss arising from the par-

ticle–wall collisions; $\vec{u}_{sw}$ refers to the slip velocity between solids and the wall; $\vec{n}$ is the unit vector pointing inward normal to the wall and $\overline{\overline{\tau}}_{sw}$ denotes the solids shear stress at the wall; q_w is the flux of granular temperature toward the wall; and e_w is the restitution coefficient of particle–wall collision.

Steady-state simulations of single-phase flows (with no particles) are first carried out. The steady-state solutions for the single-phase flows provide the initial condition for the transient two-phase flow simulations. Although transient simulations were carried out, solutions actually reached steady state after the initial transient period. The typical time step used is 1×10^{-4} s, with the temporal evolution of several flow quantities (velocity, pressure, and solid concentration profiles) being monitored at different axial locations of the pipe. The time step 10^{-4} s was chosen in such a way that it gave convergent results with a sufficient temporal resolution in a reasonable number of iterations for each time step. The results presented are in the fully developed regions, confirmed through checking the axial profile of variables (velocities, volume fraction, and pressure).

Model equations for gas-solids flow

$$\frac{\partial}{\partial t}(\rho_g \alpha_g) + \nabla \cdot (\rho_g \alpha_g \vec{u}_g) = 0 \tag{A1}$$

$$\frac{\partial}{\partial t}(\alpha_g \rho_g \vec{u}_g) + \nabla \cdot (\alpha_g \rho_g \vec{u}_g \otimes \vec{u}_g) = -\alpha_g \nabla p_g + \nabla \cdot \overline{\overline{\tau}}_g + \alpha_g \rho_g \vec{g} + \beta(\vec{u}_s - \vec{u}_g) \tag{A2}$$

$$\frac{\partial}{\partial t}(\rho_s \alpha_s) + \nabla \cdot (\rho_s \alpha_s \vec{u}_s) = 0 \tag{A3}$$

$$\frac{\partial}{\partial t}(\alpha_s \rho_s \vec{u}_s) + \nabla \cdot (\alpha_s \rho_s \vec{u}_s \otimes \vec{u}_s) = -\alpha_s \nabla p_g - \nabla p_s + \nabla \cdot \overline{\overline{\tau}}_s + \alpha_s \rho_s \vec{g} + \beta(\vec{u}_g - \vec{u}_s) \tag{A4}$$

$$\alpha_g + \alpha_s = 1 \tag{A5}$$

Interphase Transport Coefficient (Schuh et al., 1989)

$$\beta = \frac{\alpha_s \rho_s f}{T_s} \tag{A6}$$

where

$$T_s = \frac{\rho_s d_s^2}{18 \mu_g} \qquad f = \frac{C_D \mathrm{Re}_s}{24} \qquad \mathrm{Re}_s = \frac{\rho_g d_s |\vec{u}_s - \vec{u}_g|}{\mu_g}$$

$$C_D = \begin{cases} 24(1 + 0.15\ \mathrm{Re}_s^{0.687})/\mathrm{Re}_s & 0 < \mathrm{Re}_s \le 200 \\ 24(0.914\ \mathrm{Re}_s^{0.282} + 0.0135\ \mathrm{Re}_s)/\mathrm{Re}_s & 200 < \mathrm{Re}_s \le 2500 \\ 0.4008 & \mathrm{Re}_s > 2500 \end{cases}$$

Gas-Phase Stress

$$\overline{\overline{\tau}}_g = 2\alpha_g \mu_{eff,g} \overline{\overline{S}}_g \tag{A7}$$

where

$$\overline{\overline{S}}_g = \tfrac{1}{2}[\nabla \vec{u}_g + (\nabla \vec{u}_g)^T] - \tfrac{1}{3}(\nabla \cdot \vec{u}_g)\bar{\bar{I}}$$

$$\mu_{eff,g} = \mu_{g,e} + \mu_t \tag{A8}$$

$$\mu_{g,e} = \mu_g(1 + 2.5\alpha_s + 7.6\alpha_s^2)\left(1 - \frac{\alpha_s}{\alpha_{s,\max}}\right) \tag{A9}$$

$$\mu_t = \rho_g C_\mu \frac{\kappa^2}{\varepsilon} \tag{A10}$$

Turbulence Model

$$\frac{\partial}{\partial t}(\alpha_g \rho_g Y) + \nabla \cdot (\alpha_g \rho_g \vec{u}_g Y) = \nabla \cdot \left(\alpha_g \frac{\mu_{eff,g}}{\sigma_Y} \nabla Y\right) + S_{Y1} + S_{Y2} \tag{A11}$$

where Y stands for either κ or ε.

$$S_{k1} = \alpha_g(G_k - \rho_g \varepsilon) \qquad S_{\varepsilon 1} = \alpha_g \frac{\varepsilon}{\kappa}(C_{1\varepsilon} G_k - C_{2\varepsilon} \rho_g \varepsilon) \tag{A12}$$

$$G_k = \mu_t \left(\frac{\partial u_{gi}}{\partial x_j} + \frac{\partial u_{gj}}{\partial x_i}\right) \frac{\partial u_{gi}}{\partial x_j}$$

$$S_{k2} = -\beta \overline{\vec{u}_g' \cdot (\vec{u}_g' - \vec{u}_s')} = -\beta(2\kappa - \overline{\vec{u}_g' \cdot \vec{u}_s'})$$

$$S_{\varepsilon 2} = -C_{2\varepsilon} \frac{\varepsilon}{\kappa} s_{\kappa 2} \tag{A13}$$

$$\overline{\vec{u}_g' \vec{u}_s'} \le \sqrt{\overline{(\vec{u}_g')^2}\,\overline{(\vec{u}_s')^2}} = \sqrt{2\kappa}\ \sqrt{3\Theta_s} \qquad \text{(Mallo, 1997)} \tag{A14}$$

Solid Stress

$$\overline{\overline{\tau}}_s = \alpha_s \mu_b \nabla \cdot \vec{u}_s \bar{\bar{I}} + 2\alpha_s \mu_{ss} \overline{\overline{S}}_s \tag{A15}$$

$$\overline{\overline{S}}_S = \tfrac{1}{2}[\nabla \vec{u}_S + (\nabla \vec{u}_S)^T] - \tfrac{1}{3}(\nabla \cdot \vec{u}_S)\bar{\bar{I}} \tag{A16}$$

$$\mu_b = \frac{4}{3} \alpha_s \rho_s d_s g_0 (1 + e_s)\left(\frac{\Theta_s}{\pi}\right)^{1/2} \tag{A17}$$

$$\mu_s = \mu_{s,col} + \mu_{s,kin} \tag{A18}$$

$$\mu_{s,col} = \frac{5\rho_s d_s (\Theta_s \pi)^{1/2}}{96\alpha_s}\left\{\left[\frac{8\alpha_s}{5(2-\eta)}\right] \times \left[1 + \frac{8}{5}\eta(3\eta - 2)\alpha_s g_0\right] + \frac{768}{25\pi}\eta\alpha_s^2 g_0\right\} \tag{A19}$$

$$\mu_{s,kin} = \frac{5\rho_s d_s(\Theta_s\pi)^{1/2}}{96\alpha_s\eta(2-\eta)g_0}\left\{\left(\frac{1}{1+\frac{\zeta}{R}}\right)\times\left[1+\frac{8}{5}\eta(3\eta-2)\alpha_s g_0\right]\right\} \quad \text{(A20)}$$

$$g_0 = \left[1-\left(\frac{\alpha_s}{\alpha_{s,\max}}\right)^{1/3}\right]^{-1} \quad \text{(A21)}$$

$$\eta = \frac{1+e_s}{2} \quad \text{(A22)}$$

$$\zeta = \frac{d_s}{6\sqrt{2}\,\alpha_s} \quad \text{(A23)}$$

Granular Temperature

$$\frac{3}{2}\left[\frac{\partial}{\partial t}(\rho_s\alpha_s\Theta_s)+\nabla\cdot(\rho_s\alpha_s\vec{u_s}\Theta_s)\right] = (-p_s\bar{\bar{I}}+\bar{\bar{\tau}}_s):\nabla\vec{u_s}+\nabla\cdot(k_s\nabla\Theta_s)-\gamma_s+\varphi_{sg} \quad \text{(A24)}$$

$$p_s = \rho_s\left(\frac{\alpha_s}{1+\frac{\zeta}{R}}+4\eta\alpha_s^2 g_0\right)\Theta_s \quad \text{(A25)}$$

$$k_s = \frac{25\sqrt{\pi}}{128}\rho_s d_s\left\{\left(\frac{1}{1+\frac{\zeta}{R}}\frac{8}{\eta g_0}+\frac{96\alpha_s}{5}\right)\times\left[\frac{1+\frac{12}{5}\eta^2(4\eta-3)\alpha_s g_0}{41-33\eta}\right]+\frac{512}{25\pi}\eta\alpha_s^2 g_0\right\}\sqrt{\Theta_s} \quad \text{(A26)}$$

$$\gamma_s = 3(1-e_s^2)\alpha_s^2\rho_s g_0\Theta_s\left(\frac{4}{d_s}\sqrt{\frac{\Theta_s}{\pi}}-\nabla\cdot\vec{u_s}\right) \quad \text{(A27)}$$

$$\varphi_{sg} = -\beta(3\Theta_s-\sqrt{2k}\,\sqrt{3\Theta_s}) \quad \text{(A28)}$$

Boundary Conditions

$$\frac{\vec{u_{sw}}\cdot\bar{\bar{\tau}}_{sw}\cdot\vec{n}}{|\vec{u_{sw}}|} = \frac{\pi\rho_s|\vec{u_{sw}}|\phi\sqrt{\Theta_s}}{2\sqrt{3}\left(\frac{\alpha_{s,\max}}{\alpha_s}-\frac{\alpha_{s,\max}^{2/3}}{\alpha_s^{2/3}}\right)} \quad \text{(A29)}$$

$$q_w+\frac{\pi\rho_s\vec{u_s}\cdot\vec{u_s}\phi\sqrt{\Theta_s}}{2\sqrt{3}\left(\frac{\alpha_{s,\max}}{\alpha_s}-\frac{\alpha_{s,\max}^{2/3}}{\alpha_s^{2/3}}\right)}-\frac{\sqrt{3}\,\pi\rho_s(1-e_w^2)\Theta_s^{3/2}}{4\left(\frac{\alpha_{s,\max}}{\alpha_s}-\frac{\alpha_{s,\max}^{2/3}}{\alpha_s^{2/3}}\right)}=0 \quad \text{(A30)}$$

Manuscript received Mar. 15, 2003, and revision received Nov. 5, 2003.